IEICE TRANS. FUNDAMENTALS, VOL.E93–A, NO.8 AUGUST 2010

PAPER

A Computer-Aided Distinction Method of Borderline Grades of Oral Cancer

Mustafa M. SAMI[†a)], **Masahisa SAITO**[††], ***Student Members***, **Shogo MURAMATSU**[†], ***Member***, **Hisakazu KIKUCHI**[†], ***Fellow***, ***and*** **Takashi SAKU**[†††], ***Nonmember***

SUMMARY We have developed a new computer-aided diagnostic system for differentiating oral borderline malignancies in hematoxylin-eosin stained microscopic images. Epithelial dysplasia and carcinoma in-situ (CIS) of oral mucosa are two different borderline grades similar to each other, and it is difficult to distinguish between them. A new image processing and analysis method has been applied to a variety of histopathological features and shows the possibility for differentiating the oral cancer borderline grades automatically. The method is based on comparing the drop-shape similarity level in a particular manually selected pair of neighboring rete ridges. It was found that the considered similarity level in dysplasia was higher than those in epithelial CIS, of which pathological diagnoses were conventionally made by pathologists. The developed image processing method showed a good promise for the computer-aided pathological assessment of oral borderline malignancy differentiation in clinical practice.

key words: *medical image analysis, oral borderline malignancy, feature quantification, segmentation, edgel*

1. Introduction

Oral cancer is one of the six most common human cancers in the world. In many Asian and Arabic cultures, the chewing habit (e.g. Qat, betel, and paan) is known to be an important risk factor for developing oral cancer. In Yemen and India, oral cancers are the most common, representing up to 30% of all body cancers. Oral cancers have been considered to develop from their pre-malignant lesions, such as leukoplakia, which histopathologically includes two major borderline malignancies: epithelial dysplasia and carcinoma in-situ (CIS).

Since it is still difficult for pathologists to make a proper diagnosis of these borderline malignancies only on hematoxylin-eosin stained specimens [1], computer-aided diagnostic tools can be developed for objective analysis of microscopic images of oral tissues [2]. The oral dysplasia and CIS are two different grades, which should be distinguished from each other, because CIS develops into invasive squamous cell carcinoma. However, it is not always clear for pathologists how to differentiate them due to their histological similarities [3], [4]. Accurate histopathological grading necessitates different treatments, making such a diagnostic decision a complicated responsibility for pathologists.

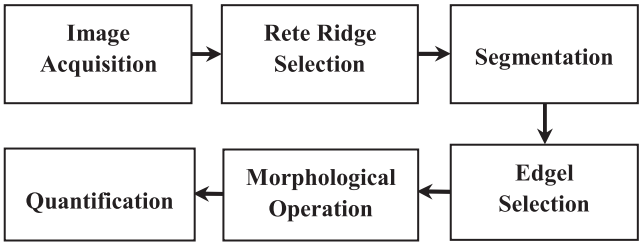

Fig. 1 The main schematic structure of the method.

In this paper, our aim is to present a new method that enables the distinction of CIS from dysplastic epithelia based on the analysis of drop variations of rete ridge units. Our approach can be divided into several well-defined stages as illustrated in Fig. 1.

After image acquisition using a high resolution digital camera, the best matching pair of neighboring rete ridges is selected among the other rete ridges presented in the same tissue section. This criterion of malignancy that has been considered will be covered in details in Sect. 2.

Followed to feature selection, a feature extraction method is developed in order to extract the contour of the rete ridges. This was achieved by applying saturation based color segmentation in the HSV color space with the purpose of separating the epithelium region from the rest of the tissue image. After segmentation, a texture-based operation has been concerned in which the main pixels at the border of the objects are defined and referred to as edgels. Next, a morphological operation based on dilation is applied followed by a thinning operation to connect the edgels. A chain coding is designed to trace the contour that represents the rete process contour. The details of the method are described in Sect. 3, while Sect. 4 describes the quantification part. The obtained results are shown in Sect. 5. Finally, a discussion and some concluding remarks are given in Sects. 6 and 7, respectively.

2. Histological Features of Borderline Malignancies

Observing histological changes under the microscope is still

Manuscript received November 18, 2009.
Manuscript revised February 28, 2010.

[†]The authors are with the Department of Electrical and Electronic Engineering, Niigata University, Niigata-shi, 950-2181 Japan.
[††]The author is with Imaging Science and Engineering Laboratory, Tokyo Institute of Technology, Yokohama-shi, 226-8503 Japan.
[†††]The author is with Division of Oral Pathology, Graduate School of Medical and Dental Sciences, Niigata University, Niigata-shi, 951-8514 Japan.
a) E-mail: mustafa@telecom0.eng.niigata-u.ac.jp

DOI: 10.1587/transfun.E93.A.1544

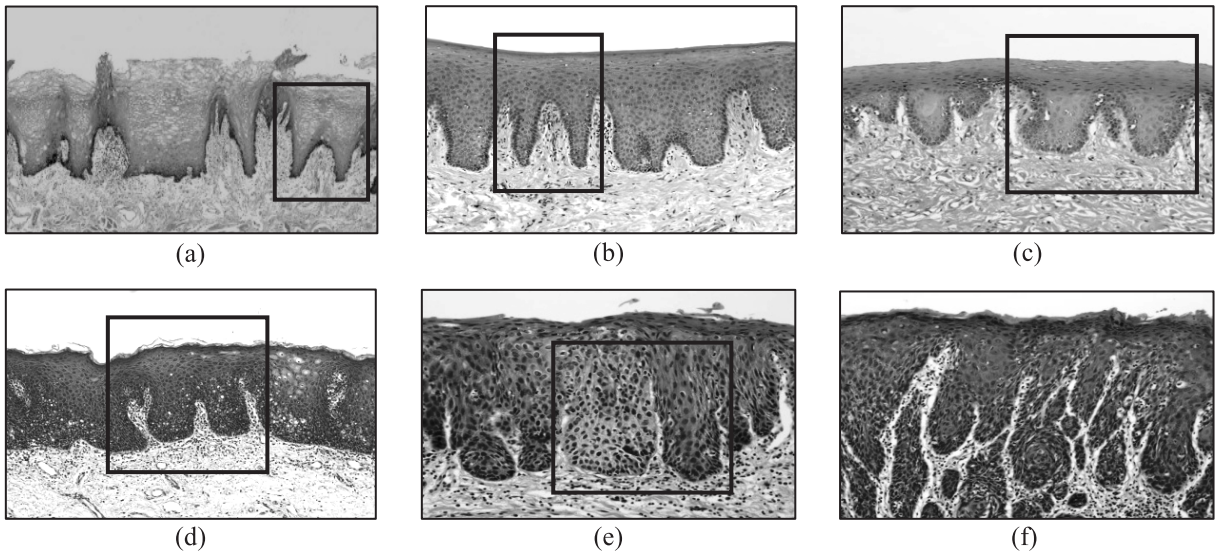

Fig. 2 Varieties of rete ridges among oral epithelial lesions. (a) Normal epithelium. (b) Epithelial hyperplasia. (c) Epithelial dysplasia. (d) Carcinoma in-situ. (e) Carcinoma in-situ with micro-invasion. (f) Invasive squamous cell carcinoma.

an essential practice in the oral cancer diagnosis. Pathologists evaluate those changes in regards to how they are different from their normal appearances.

This section explains some basic concepts on how pathologists make their diagnostic decisions under the microscope, although it is not the aim of this article to explain it in detail that could be found in histopathological papers [1]. The criteria used for grading epithelial dysplasia in the WHO 2005 classification [5] included seven architectural and nine cytological criteria. One of the most important architectural changes must be alteration of the rete ridges, and hence we first adopted analysis of the rete ridge shape when seeking histological objects to be investigated by a computer-aided method. The rete ridge shape or contour can be defined as the edge segment that separates the epithelium region from the connective tissue. Thus, the shape of rete ridges (projection parts of the covering epithelium, also known as rete processes or rete pegs) is a histological key feature highly considered by pathologists for differentiating grades of the oral borderline malignancies [1], [6].

In contrast to normal rete ridges, those towards malignant transformation become enlarged down in the direction of underlying connective tissues. The most characteristic form at this stage is a drop-shape, which was basically indicated by the WHO classification [5], [6]. Figure 2 shows the representative rete ridge variations selected from oral mucosal lesion samples whose diagnoses were well agreed upon by different pathologists. However, carcinoma in-situ (Fig. 2(d)) is not always clearly identified from epithelial dysplasia (Fig. 2(c)). Since these borderline malignancy lesions resemble each other, their diagnosis requires extra attention by pathologists [1]. The marked rete ridge pairs in Fig. 2 are of particular importance and this will be explained later in this section.

As shown in Fig. 2(a), normal rete ridges are random-

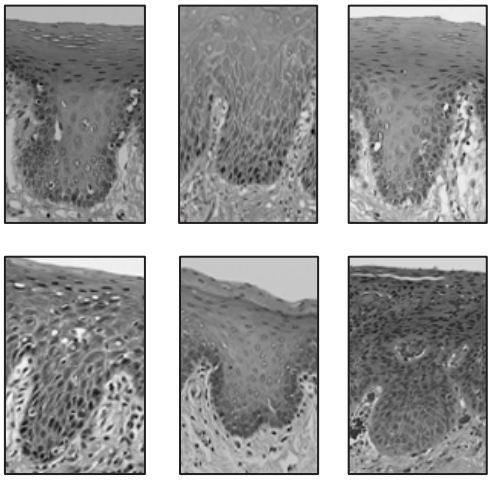

Fig. 3 Representative rete ridges of oral borderline malignancies. Panels in the upper row show those of epithelial dysplasia and those in the lower row are those of carcinoma in-situ.

shaped and project in slightly different directions. When they change their shapes in the process of malignant transformation, it becomes a hard and subjective task to make diagnostic decisions only by the pathologists' eyes [4]. This is because pathologists must evaluate individual rete ridges as well as their whole tendencies of alteration. Figure 3 shows representative examples of drop-shape rete ridges which are frequently seen in epithelial dysplasia and CIS. Therefore, it was difficult to discriminate CIS from epithelial dysplasia, as far as only the individual drop shape of rete ridges is concerned. In this study, we have thus focused our attention to these drop shapes swelling of rete ridges. Our concern was how to distinguish them by objective ways. To this end, we have invented a new diagnostic method by using immunohistochemistry [7] that leads to reasonable distinction

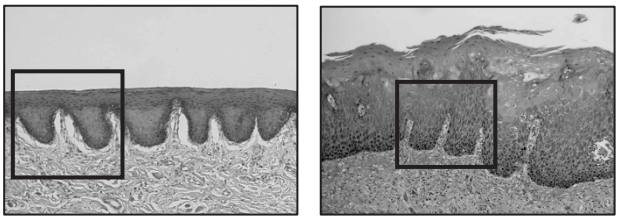

Fig. 4 Twin rete ridges. (a) Best match twin rete ridges. (b) Standalone twin rete ridges.

of borderline grades based on the current biological concept of cellular differentiation and proliferation [8], [9].

In the daily practice of surgical pathology, it is common to observe multiple neighboring rete ridges similar to each other at a glance. Applying this visual behavior to our image acquisition, we pick up two neighboring rete ridges as a unit and called them *twins* as shown in Fig. 4. It is assumed that, in normal epithelia the twin rete ridges should have the maximum similarity appearance (Fig. 2(a)). When normal rete ridges start to change their shapes towards malignant transformation, each rete ridge of the twins would start to deform itself and obtain its own new shape independently at different speeds and in different directions. Thus, the similarity between the twin mates would decrease with respect to malignancy levels. The twin rete ridges could be divided into two main categories; either the best matching pair of rete ridges next to each other among all rete ridges as shown in Fig. 4(a), or a standalone pair of rete ridges as shown in Fig. 4(b).

Based on the current understanding in cancer research, it is important to note that cancer is a genetic disease which is generated by gene mutation in singular or a small number of cells. In their process of proliferation, cancer cells would start to communicate with their neighboring cells [10], [11], and this should cause an autonomous and excessive growth, resulting in an enlargement of the rete ridges of the oral epithelia. Therefore, the likelihood that twin rete ridges are within the same grade is very high, since they started the cancerous growths at a similar time.

The above mentioned is our hypothesis for the present paper, and our method is basically a shape comparison between those neighboring rete ridges.

3. Materials and Method

3.1 Origin and Acquisition

All biopsy samples were prepared by using the standard pathological procedure. Tissue sections were cut by a microtome at 5 μm thick. These sections were stained with hematoxylin and eosin (HE). Eighteen histological features of rete ridges from 6 normal and 6 dysplastic epithelia and 6 CIS, collected from different sites of the oral mucosa including the lips, tongue, gingiva, palate, floor of the mouth, and buccal mucosa but not from atrophic types epithelial dysplasia or CIS, which have no obvious rete ridges. The histopathological criteria for epithelial dysplasia and CIS of the oral mucosa were described elsewhere [1], [12]. We selected epithelial dysplasia cases with the characteristic two-phase appearance in which the presence of proliferating centers was confirmed in HE stain and immunohistochemical stain for Ki-67 [13]. For the diagnosis of CIS, we chose cases with the typical histology for the three variations, basaloid, verrucous, and acanthotic types, with an aid of immunohistochemical stainings for keratin 13, keratin 17, keratin 19, and Ki-67 [12]. The 18 cases mentioned above were selected from the surgical pathology file at the Division of Oral Pathology, Niigata University, Graduate School of Medical and Dental Sciences, during one-year period of 2008, in which 96 cases of epithelial dysplasia and 54 cases of CIS were registered in addition to 97 cases of squamous cell carcinomas and more than 180 cases of the other lesions containing normal squamous epithelia. Their HE-stained sections together with immunohistochemical ones were circulated among the oral pathologists at authors' and a few overseas institutions for reconfirming their diagnoses. Only those samples of which diagnoses were agreed by at least three pathologists were selected and captured on a high quality optical microscope (Nikon S-800, Tokyo, Japan) equipped with a high resolution digital camera (Nikon DXM1200C). Every image was acquired with the magnifications at 20× and 2058 × 1536-pixel resolution on the camera. The image files captured by the pathologist author were saved in TIFF format and delivered to the engineer authors for further investigations.

The intensity level was adjusted in such a way that digitized images become visually acceptable by pathologists. The rotation of the captured images was to be set in a way that the upper surface of the epithelium was in a horizontal position if at all possible.

3.2 Twins Selection

By using the developed graphical user interface (GUI), at a glance the region of interest (ROI) where the twin rete ridge is selected by specifying a cropped rectangle that fits the twin area in the image as shown in Fig. 4. The rest of other distinction processes are applied to the ROI automatically.

3.3 Epithelium Segmentation

In this study we must extract the targeted histological feature, the rete processes, in order to quantify the drop-shape similarity between the twin rete ridges. The rete process is an edge segment that can be obtained from the boundary pixels of the epithelium region. Thus, epithelium segmentation is a crucial step in this study with some challenges. The challenges are mainly from staining artifacts, lighting acquisition conditions, and undesired touching objects.

In past literature, epithelium segmentation and rete process extraction were targeted in different studies [14], [15]. Here, we have developed a new method for epithelium seg-

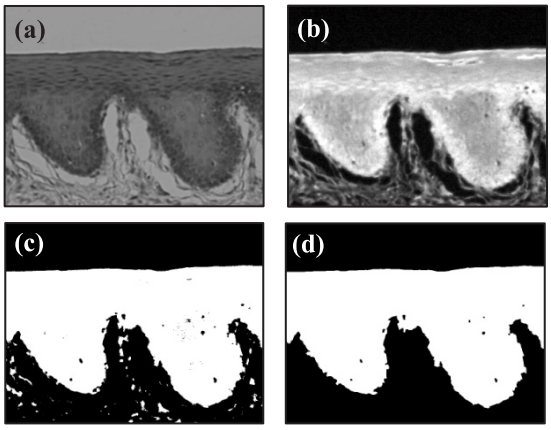

Fig. 5 Epithelium segmentation. (a) Twins ROI. (b) Adjusted saturation component. (c) Morphed image. (d) Largest region.

mentation and rete processes representation [16], [17]. The method was developed based on the assumption that an HSV representation has a certain advantage over RGB when it comes to epithelium segmentation. The HSV color system is considerably closer than the RGB system to the way in which humans experience and perceive color sensations [18]. The saturation component in the epithelium region has a lower saturation than the connective tissue. The intensity has been adjusted over the saturation component in such a way that 1% of the intensity values are saturated at low and high intensities. Pixels with low intensity values will be replaced in a lower intensity, and pixels with high intensity values will be replaced in a higher intensity. This increases the contrast in the image as shown in Fig. 5(b).

A global thresholding based on the Otsu method [19] has been used to determine the threshold value applied to the adjusted saturation component of the HSV color space. It creates a bilevel image based on the quantization of intensity values of the saturation component image. Pixels with intensity values falling within a given range are determined as foreground (ones), while all other pixels are determined as background (zeros). With respect to the image in Fig. 5(c), the threshold value obtained from Otsu's method is 0.55. The undesired occlusion objects were removed by applying morphological operations.

At first, the objects in the obtained bilevel image are thickened by adding pixels to the exterior of the objects until doing so would result in previously unconnected objects being 8-connected. Note that a pixel is said to be 8-connected, if it is connected to at least one of 8 immediate neighbors. Similarly, a pixel is said to be 4-connected, if it has at least one unit-distance neighbor along the horizontal and vertical directions. The resultant image from this thickening is referred to as I. Separately, the binary image objects will be bridged in order to connect the objects separated by a single pixel gaps, and we will call this image J. Both the thickened and the bridged images will be added together $I + J$ and this will assure us that the closest objects near to the epithelium are joined into the epithelium and only those objects relatively far away are discarded.

The above mentioned thickening [18] of a bilevel image A is defined as

$$A \odot B = A \cup (A * B) \tag{1}$$

where $\cup$ denotes the union of two sets. B is a pair of structuring elements, $B = (B_1 + B_2)$, used in the hit-or-miss transformation [18] in such a way that

$$A * B = (A \ominus B_1) \cap (A^c \ominus B_2) \tag{2}$$

where $\cap$ stands for the intersection of two sets. AB_1 indicates the erosion of A by B_1 and A^c is the background of A.

A morphological opening operation using a 3×3 square structuring element is applied to the image, $I + J$. Morphological opening is the erosion of A by B followed by dilation by B. The erosion of A by B is defined as

$$A \ominus B = \{z|(B)_z \cap A^c \neq \phi\} \tag{3}$$

where $(B)_z$ denotes the structuring element B translated by z and ϕ is the empty set. The dilation of A by B is expressed by

$$A \oplus B = \{z|(\hat{B})_z \cap A \neq \phi\} \tag{4}$$

where $(\hat{B})_z$ stands for the translation of B by z of the reflection about the origin.

The largest region (here it is the epithelium) is targeted, while all the other objects will be removed by labeling the regions to get the region that has the largest area. The image is then to be closed by a morphological closing operation (dilation followed by erosion) using the same 3×3 square structuring element. The obtained result is shown in Fig. 5(d). The whole sequence of the described operations is demonstrated in Fig. 6.

3.4 Contour Extraction of Rete Processes

3.4.1 Selection of Wide-Angle Edgels

The epithelium boundary is disconnected and fragmented because of insufficient contrast and imperfect segmentation. For a precise extraction of contour pixels of an epithelium that can possibly represent the rete processes, we used highly textured areas in this work known as wide-angle edgel method [20]. One of its advantages is that the boundary of an object is detected, even if the object boundary may be disconnected. Edgels are edge pixels located at the boundary of an object. The method can be explained as follows. If someone takes a position at the front edge of an object, he or she will see nothing in the field of view within the line-of-sight distance.

In part (a), P is to be checked if it is an edgel, and it is assumed that five significant pixels, A, B, C, D, and E, are present within a line-of-sight distance. The line-of-sight distance is defined by a 7×7 window located at P. Two

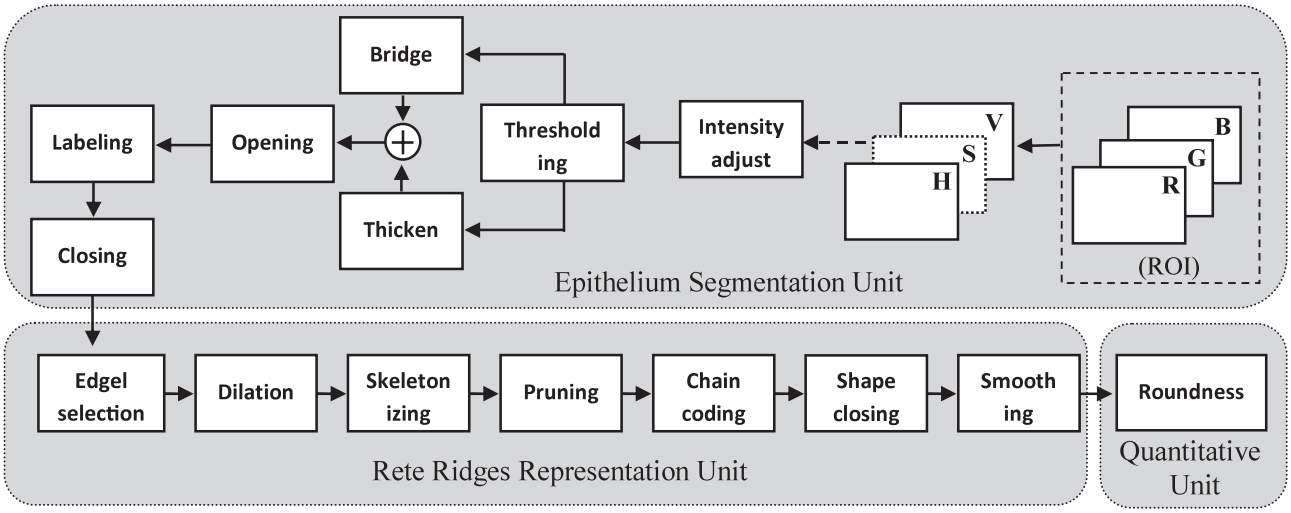

Fig. 6 The sequence of the different operations used by the computer-aided diagnostic system.

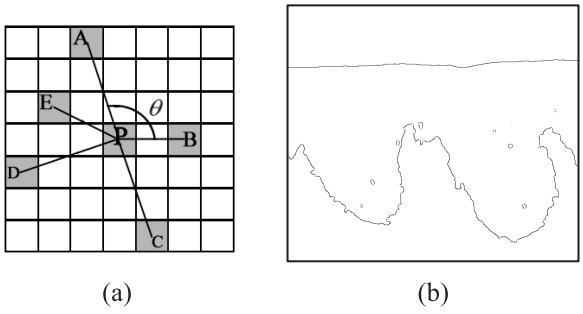

Fig. 7 Wide-angle edgel method. (a) Wide-angle edgel window. (b) The obtained edgels from the method.

successive significant pixels are visited in the clockwise order to define a field of view with respect to P. If there is a field-of-view angle that is wider than or equal to 90 degrees, P is identified as an edgel. This condition is easily checked by the inner product. For any pair of points, say A and B, a pair of vectors, a and b, is defined with respect to P in such a way that they are outgoing vectors from P. The inner product between a and b is written by

$$\langle a, b\rangle = |a| \cdot |b| \cos\theta, \tag{5}$$

where θ is $\angle$APB. If the inner product is not positive, P is an edgel. The obtained result is shown in Fig. 7(b).

3.4.2 Connecting Edgels

The targeted contour must satisfy two conditions; to be continuous and to be of one-pixel thickness. The image obtained from the wide-angle edgel method consists of sparse edgel pixels and is considered to represent the main shape of the rete process contour. The gap between pixels is filled by a dilation operation using a 4×4 square structuring element to connect the edgel pixels. The size of the structuring element is sufficient to fill the maximum gap between edgels obtained from a 7×7 window.

3.4.3 Skeletonization

Skeletonization thinning method [21] is applied to the image. Different skeletonizing algorithms can be found in the literature and they produce slightly different skeletons [22]. The skeletonization will remove pixels on the boundaries of objects but does not allow objects to break apart. Skeleton can be defined as conditional erosion under the following conditions: do not remove a single pixel, do not break the connectivity, and do not remove an endpoint pixel. This process is applied iteratively, until the image no longer changes. If a pixel has at most a single neighbor with respect to either 4 or 8-connectivity, it is an endpoint.

For our application, the requirements for the contour skeleton are: 1) the resulting skeleton must be topologically equivalent to the object; 2) it must be one pixel-thick; 3) it must be connected in terms of the 8-connectivity. Note that if a pixel has at least one neighboring pixel among 8 possible locations with respect to the 8-connectivity, it is identified to be connected. The skeleton of A is expressed in terms of erosions and openings [18] and is written as

$$S(A) = \bigcup_{k=0}^{K} S_k(A) \tag{6}$$

with

$$S_k(A) = (A \ominus kB) - (A \ominus kB) \circ B \tag{7}$$

where $\circ$ indicates morphological opening and B is a structuring element, and $A \ominus kB$ indicates k successive erosions of A by B. K is given by

$$K = \max\{k | (A \ominus kB) \neq \phi\} \tag{8}$$

It expresses the maximum count of iterations before A may have eroded to an empty set. The obtained image from this skeletonization is shown in Fig. 8(a). It is interesting to note

Fig. 8 Skeletonizing and Pruning. (a) Skeletonized image. (b) Chain coding output contour.

that the skeleton defined by Eq. (6) allows itself to reconstruct the original image, as follows.

$$A = \bigcup_{k=0}^{K} (S_k(A) \oplus kB) \tag{9}$$

where $S_k(A) \oplus kB$ indicates k successive dilations of $S_k(A)$ by B.

3.4.4 Pruning

The obtained skeletons usually contain spurious arcs that are not topologically part of the targeted feature, the rete processes edge. In our case, the length of the spurious arcs is not important, so all of these arcs must be removed. An easy way to remove those arcs is to keep eliminating the endpoint pixels iteratively until doing so will make no change in the image between two consecutive iterations. Pixels touching the boundaries of the image are not considered to be endpoints.

3.4.5 Chain Coding

Finally, we have designed a chain coding for our application to facilitate tracing the connected pixel contour that represents the rete processes. The starting point is always determined by the pixel located in the bottom leftmost of the first column of the image, and it can be identified by the highest value of the y-axis coordinate. Going forward to the rightmost end of the image can be obtained by checking all the possible pixels after every movement. Inside a 3×3 window size, the movement priority of the chain code is always given to the next south side pixel. The obtained rete processes edge is shown in Fig. 8(b).

3.5 Shape Closing and Smoothing

Each rete ridge unit is determined by finding the upper peak-points of the rete process that appears at every 1/3 part of the image width. Finding these peak-points located in the innermost edge of the rete ridges was obtained by dividing the image vertically into three equal parts; P_1, P_2, and P_3. In a normal coordinate convention, checking the x-y coordinates of all contour pixels was done to find the four innermost pixels of the rete ridge units using the following steps:

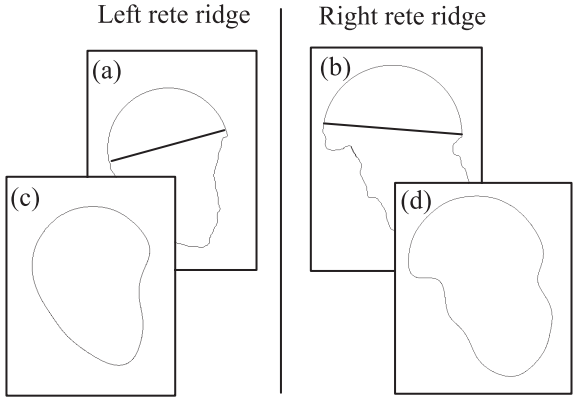

Fig. 9 Rete ridge unit representation. (a-b) The added half circle arc at the innermost upper peak-pints. (c-d) The smoothed contours using 2% of the descriptors.

1) in P_1 select the lowest y-axis pixel that has the highest x-axis; 2) in P_2 select the lowest y-axis pixel that has the lowest x-axis; 3) in P_2 select the lowest y-axis pixel that has the highest x-axis; 4) in P_3 select the lowest y-axis pixel that has the lowest x-axis.

The two innermost peak-point pixels for the left side rete ridge unit are determined from step 1 and 2. While the other two innermost peak-point pixels for the right side rete ridge unit are determined from step 3 and 4. A half circle arc is then added to the rete ridge segment in order to obtain a closed loop shape that could represent one rete ridge unit as illustrated in Figs. 9(a) and (b).

Smoothing the obtained closed-loop contour has been done by reducing the number of contour descriptors. For images captured under the acquisition conditions described in Sect. 3.1, 2% of the descriptors were enough to obtain a more regular shape for representing every rete ridge unit.

Shape smoothing by reducing the number of Fourier coefficients is a well-known technique in image processing and has been used in different applications [18], [23].

Assume that the contour of a shape consists of N points of which horizontal and vertical coordinates are written by $x(n)$ and $y(n)$, respectively, for $n = [0, N-1]$. The Fourier descriptor of the contour is defined by the discrete Fourier transform as follows.

$$D(k) = \sum_{n=0}^{N-1} W^{-kn} d(n), \tag{10}$$

where

$$d(n) = x(n) + jy(n), \text{ and } W = e^{j\frac{2\pi}{N}}$$

An approximate description of the contour is obtained by keeping M low-frequency components as they are and by neglecting the other high-frequency components, where $M < N$. A smoothed description of the contour is given by

$$\hat{d}(n) = \frac{1}{N} \sum_{k=0}^{N-1} W^{nk} \hat{D}(k), \tag{11}$$

where

$$\hat{D}(k) = \begin{cases} 0, & \text{if } \left\lfloor \frac{M}{2} \right\rfloor < k < N - \left\lfloor \frac{M-1}{2} \right\rfloor \\ D(k), & \text{otherwise.} \end{cases} \quad (12)$$

$\lfloor a \rfloor$ denotes the maximum integer that does not exceed a.

The contour of the image in Fig. 9(a) consists of $N = 858$ points in total and has been reduced to its 2% of descriptors. The resulting smoothed contours are shown in Figs. 9(c) and (d).

4. Quantification

The aim of the developed image processing method is to measure the drop-shape development in order to compare the malignancy level of the twin rete ridges. Shape factors are a set of equations used to quantify the shape roughness in different applications [23], [24]. The measurement of roundness was the shape factor used to quantify the drop-shape level [23]. The roundness of an object is defined by

$$R = \frac{A}{\pi r^2} \quad (13)$$

where A and r denote the area and a half the maximum diameter of the object, respectively. The roundness is scale and rotation-invariant. Hence it offers an objective and robust metric against possible variations in orientation, size, and shape.

5. Results

Table 1 shows part of the results for 6 tested images so as to describe the way of analysis that has been used. Each tissue sample image contains at least a single twin pair rete ridges indicated as left and right. The higher value of roundness of the twin mates from either side was selected to indicate the maximum malignancy level that has been developed (shown in *italic*). Simultaneously, the absolute difference value between the twins mate's roundness was used to show the drop-shape similarity level (shown in **bold**). In the same way, Fig. 10 shows the distribution of the whole tested samples in a feature space where three clusters of normal, dysplasia, and CIS samples are found to be clearly separated. Each mark in the plot represents a pair of rete ridge twins. The roundness similarity level is measured along the x-axis and the maximum malignancy level is in the y-axis.

6. Discussions

We have developed the software package with the name TwinsViewer that implements the diagnostic system described in this paper [25]. A user friendly front-end GUI has been designed in order to aid pathologists in examining the drop-shape similarity between the twin rete ridges. After specifying a pair of targeted twins, the rest of the procedure is automatic. In this paper, the tested images were selected from different parts of oral malignancy. The developed image processing method shows success for epithelium segmentation and rete processes representation in the HE stained oral microscopic images. The considered twin histopathological method was reasonably accepted from different pathologists since it is based on the existing fundamentals of oral histology in cancer research.

Table 1 Results for 6 test images.

Tissue Sample	Roundness		
	Left	Difference	Right
Norm1	0.23	**0.02**	*0.25*
Norm2	*0.31*	**0.03**	0.28
Dys1	0.50	**0.08**	*0.58*
Dys2	0.65	**0.10**	*0.75*
CIS1	0.62	**0.19**	*0.81*
CIS2	*0.81*	**0.15**	0.66

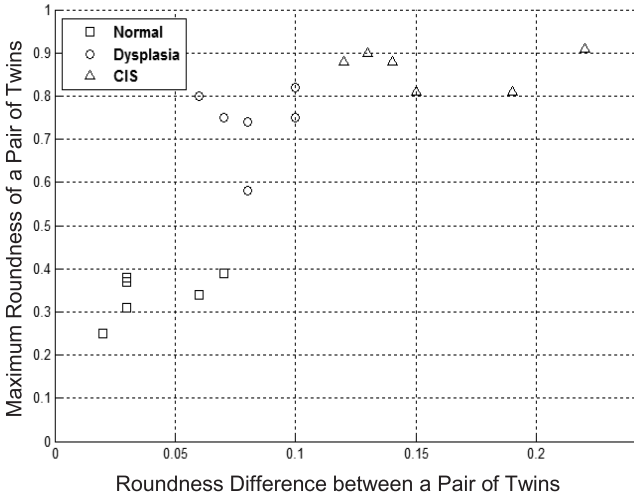

Fig. 10 Distribution of 18 tested twins samples in a two-dimensional feature space.

7. Conclusions

A new image processing method has been developed for quantifying the rete processes units in the HE stained microscopic images of the oral mucosa. The method was successful in the precise representation of the rete ridges. The drop-shape similarity between the twin rete ridges has been considered as a malignancy sign for differentiating the oral borderline grades. The measurement of roundness was the shape factor used to quantify the rete ridge units. From the obtained results, it was found the considered similarity in dysplasia was higher than those in epithelial CIS. The developed image processing method shows good promise for the computer-aided pathological assessment of oral borderline malignancy differentiation in clinical practice.

Acknowledgments

The authors would like to thank the pathologists at Divi-

sion of Oral Pathology, Niigata University, Graduate School of Medical and Dental Sciences, especially Dr. Jun Cheng, Dr. Toshihiko Mikami, and Dr. Kamal Al-Eryani for their valuable assistance to this work. They would also like to thank Dr. Faleh Sawair and Dr. Rasha Abu Eid, both from Department of Oral and Maxillofacial Surgery, University of Jordan, for their support to this work.

References

[1] T. Saku, J. Cheng, K. Komiyama, T. Kohogo, Y. Tanaka, T. Izumo, H. Hasegawa, T. Ishida, I. Ogawa, T. Takata, I. Semba, and H. Yamamoto, Guidelines for Histopathological Diagnosis of Borderline Malignancies of the Oral Mucosa, The Japanese Society of Oral Pathology, Yamazaki Publishing, Niigata, March 2005.

[2] M.M. Sami, H. Kikuchi, F. Sawair, K. Al-Eryani, and T. Saku, "Towards a computer-aided system for the histopathological diagnosis of oral borderline malignancies," AACR Int. Conf., p.115, Amman, Jordan, March 2008.

[3] A. Andrion, C. Magnani, P.G. Betta, A. Donna, F. Mollo, M. Scelsi, P. Bernardi, M. Botta, and B. Terracini, "Malignant mesothelioma of the pleura: Interobserver variability," J. Clinical Pathology, vol.48, pp.856–860, 1995.

[4] S.M. Ismail, A.B. Colclough, J.S. Dinnen, D. Eakins, D.M. Evans, E. Gradwell, J.P. O'Sullivan, J.M. Summerell, and R.G. Newcombe, "Observer variation in histopathological diagnosis and grading of cervical intraepithelial neoplasia," British Medical J., vol.298, pp.707–710, 1989.

[5] L. Barnes, J. Eveson, P. Reichart, and D. Sidransky, World Health Organization Classification of Tumours, Pathology and Genetics of Head and Neck Tumours, pp.177–179, IARC Press, Lyon, 2005.

[6] J.J. Pindborg, P.A. Reichart, C.J. Smith, I. van der Waal, "World health organization international hisological classification of tumours," in Histological Typing of Cancer and Precancer of the Oral Mucosa, 2nd ed., pp.24–27, Springer-Verlag, Berlin, 1997.

[7] M. Sami, H. Kikuchi, and T. Saku, "Quantitative analysis of the rete processes for the diagnosis of borderline malignancies in microscopic oral cancer images," 5th Int. Workshop on Computational Systems Biology, pp.149–152, Leipzig, Germany, June 2008.

[8] W. Bloom and D. Fawcett, A Textbook of Histology, W.B. Saunders, Philadelphia, 1970.

[9] N. Antonio, Ten Cate's Oral Histology: Development, Structure, and Function, Mosby, Missouri, U.S.A., 2003.

[10] H. Lodish, Molecular Cell Biology, Freeman and Company, New York, 2000.

[11] B. Alberts, A. Johnson, J. Lewis, M. Raff, K. Roberts, and P. Walter, Molecular Biology of the Cell, Taylor and Francis, New York, 2002.

[12] T. Kobayashi, H. Ida-Yonemochi, S. Maruyama, J. Cheng, M. Yagi, R. Takagi, and T. Saku, "Histopathological varieties of oral carcinoma in-situ: Diagnosis aided by immunohistochemistry, dealing with the second basal cell layer as the proliferating center of oral mucosal epithelia," Pathology International, vol.60, pp.154–164, 2010.

[13] M. Syafriadi, J. Cheng, K.Y. Jen, H. Ida-Yonemochi, M. Suzuki, and T. Saku, "Two-phase appearance of oral epithelial dysplasia resulting from focal proliferation of parabasal cells and apoptosis of prickle cells," J. Oral Pathology and Medicine, vol.34, pp.140–149, 2005.

[14] G. Landini and IE. Othman, "Estimation of tissue layer level by sequential morphological reconstruction," J. Microscopy, vol.209, no.2, pp.118–125, 2003.

[15] B. Blomgren, U. Johannesson, N. Bohm-Starke, C. Falconer, and M.A. Hilliges, "A computerized, unbiased method for epithelial measurement," Micron, vol.35, pp.319–329, 2004.

[16] M.M. Sami, H. Kikuchi, and T. Saku, "Shape analysis of the rete processes for borderline malignancies of the oral mucosal epithelia," Proc. EMBBE 2008, CD ROM, Porto, March 2008.

[17] M. Saito, H. Kikuchi, S. Muramatsu, and T. Saku, "Image processing for the aid in the diagnosis of oral pathological images," Proc. IEICE Gen. Conf. 2008, Kita Kyushu, March 2008.

[18] R.C. Gonzalez and R.E. Woods, Digital Image Processing, 2nd ed., Prentice Hall, 2002.

[19] N. Otsu, "A threshold selection method from gray-level histograms," IEEE Trans. Syst. Man. Cybern., vol.SMC-9, no.1, pp.62–66, Jan. 1979.

[20] M. Petrou and P. Sevilla, Image Processing; Dealing with Texture, John Wiley, New Jersey, 2006.

[21] C. Lantuéjoul, "Skeletonization in quantitative metallography," Issues of Digital Image Processing, R.M. Haralick and J.C. Simon, ed., NATO, Sijthoff and Noordhoff, 1980.

[22] L. Lam, S.W. Lee, and C.Y. Suen, "Thinning methodologies, a comprehensive survey," IEEE Trans. Pattern. Anal. Mach. Intell., vol.14, no.9, pp.869–885, Sept. 1992.

[23] R. Rangayyan, Biomedical Image Analysis, Taylor & Francis, New York, 2005.

[24] L. Shen, R.M. Rangayyan, and J.E.L. Desautels, "Application on shape analysis to mammographic calcification," IEEE Trans. Med. Imaging, vol.13, no.2, pp.263–274, June 1994.

[25] M.M. Sami, M. Saito, H. Kikuchi, and T. Saku, "A computer-aided distinction of borderline grades of oral cancer," IEEE ICIP 2009, pp.4205–4208, Cairo, Nov. 2009.

Mustafa M. Sami was born in Sana'a, Yemen in 1977. He received his Bachelor's degree in Electrical and Electronic Engineering from Dawood College of Engineering and Technology (DCET), Karachi, Pakistan in 2003. From 2004, he is attached with Niigata University, Niigata, where he received his Master of Engineering in 2007. He is presently working toward a Doctoral degree at the same university. He was a visiting fellow at Computational Systems Biology, Tampere University of Technology, Finland, sponsored by the Finnish government during 4 months in 2009. His research interests include digital signal processing, image processing, machine intelligence, pattern recognition and bio-imaging. He is a student member of IEEE and AACR.

Masahisa Saito was born in Shizuoka, Japan in1985. He received his B.E. degree in Electrical and Electronic Engineering from Niigata University, Niigata, and Tokyo Institute of Technology, Yokohama, in 2008 and 2010, respectively. He joined Hamamatsu Photonics, Hamamatsu in 2010. His research interest is in the field of medical imaging and medical image processing.

Shogo Muramatsu was born in Tokyo, Japan in 1970. He received B.E., M.E. and Dr.Eng. Degrees in electrical engineering from Tokyo Metropolitan University in 1933, 1995, and 1998, respectively. In 1997, He joined Tokyo Metropolitan University. In 1999, he joined Niigata University, where he is currently an Associate Professor at Department of Electrical and Electronic Engineering. He was a Visiting Researcher at MICC & VIP Laboratory University of Florence, Italy, during a year of 2003 through 2004. His research interests are in digital signal processing, multirate systems, image processing and VLSI architecture. He is a Member of ITE (Institute of Image Information and Television Engineers), IIEEJ (Institute of Image Electronics Engineers of Japan), IPSJ (Information Processing Society of Japan), and IEEE.

Hisakazu Kikuchi was born in Niigata in 1952. He received B.E. and M.E. degrees from Niigata University, Niigata, in 1974 and 1976, respectively, and Dr.Eng. degree in electrical and electronic engineering from Tokyo Institute of Technology, Tokyo, in 1988. From 1976 to 1979 he worked at Information Processing Systems Laboratory, Fujitsu Ltd., Tokyo. Since 1979, he has been with Niigata University, where he is a Professor at Department of Electrical and Electronic Engineering. During a year of 1992 to 1993, he was a visiting scholar at Electrical Engineering Department, University of California, Los Angeles, U.S.A. His research interests include digital signal processing and image/video processing. He is a Member of ITE, IIEEJ, and IEEE. He served the chair of Circuits and Systems Group, IEICE, in 2000 and the general chair of Digital Signal Processing Symposium, IEICE, in 1988 and Karuizawa Workshop on Circuits and Systems, IEICE, in 1996, respectively.

Takashi Saku was born in Fukuoka, Japan in 1950. He received a DDS degree from Tokyo Medical and Dental University, Tokyo, in 1976 and a Ph.D. degree in pathology from Kagoshima University, Kagoshima, in 1980. He was a postdoctoral associate at Yale University School of Medicine, New Haven and an assistant professor at Nagasaki University School of Dentistry, Nagasaki, and since 1990, he has been a professor of oral pathology at Niigata University Graduate School of Medical and Dental Sciences, Niigata. He served as a member of the Japanese Board of Pathology for the Certifying Examination in Oral Pathology from 2000 to 2007. Since 2007 he has been Editor-in-Chief of the Oral Medicine & Pathology.